

ARTICLE

DOI: 10.1038/s41467-018-03455-x

OPEN

The H2B deubiquitinase Usp22 promotes antibody class switch recombination by facilitating non-homologous end joining

Conglei Li¹, Thergiorry Irrazabal¹, Clare C. So¹, Maribel Berru¹, Likun Du², Evelyn Lam¹, Alexandra K. Ling¹, Jennifer L. Gommerman¹, Qiang Pan-Hammarström^{1,2} & Alberto Martin¹

Class switch recombination (CSR) has a fundamental function during humoral immune response and involves the induction and subsequent repair of DNA breaks in the immunoglobulin (Ig) switch regions. Here we show the role of Usp22, the SAGA complex deubiquitinase that removes ubiquitin from H2B-K120, in the repair of programmed DNA breaks *in vivo*. Ablation of Usp22 in primary B cells results in defects in γ H2AX and impairs the classical non-homologous end joining (c-NHEJ), affecting both V(D)J recombination and CSR. Surprisingly, Usp22 depletion causes defects in CSR to various Ig isotypes, but not IgA. We further demonstrate that IgG CSR primarily relies on c-NHEJ, whereas CSR to IgA is more reliant on the alternative end joining pathway, indicating that CSR to different isotypes involves distinct DNA repair pathways. Hence, Usp22 is the first deubiquitinase reported to regulate both V(D)J recombination and CSR *in vivo* by facilitating c-NHEJ.

¹Department of Immunology, University of Toronto, Toronto, Ontario, Canada M5S 1A8. ²Department of Laboratory Medicine, Karolinska Institutet, Stockholm SE14186, Sweden. Correspondence and requests for materials should be addressed to A.M. (email: alberto.martin@utoronto.ca)

Antibody diversification is essential for vertebrates to prevent and eradicate infections^{1–3}. Primary diversification, i.e., V(D)J recombination, creates the primary antibody repertoire and forms the antigen binding domain of the antibody¹. This process involves the generation and subsequent repair of RAG1/2-induced double-stranded DNA breaks (DSBs) at specific recombination signal sequences that flank each V, D, and J coding segment within the variable region¹. Successful V(D)J rearrangement is essential for expression of the B-cell receptor (BCR) and progression through B-cell development¹. Class switch recombination (CSR) is a secondary diversification process that drives the generation of antibodies of various isotypes (e.g., from IgM to IgG or IgA)^{2,3}. The isotype of an antibody controls its effector functions. CSR is initiated by activation-induced deaminase (AID), which catalyzes the deamination of deoxycytidines (i.e., dC→dU) in the switch regions that are upstream of each constant region within the immunoglobulin heavy chain locus, leading to a dU:dG mismatch^{3,4}. This mismatch is further processed by the mismatch repair and base excision repair pathways, resulting in the production of staggered DSBs⁵.

DSBs initiated by either RAG1/2 or AID induce a cascade of DNA damage signaling, in which phosphorylation of H2AX on serine 139 (γ H2AX) has a critical function by recruiting various DNA repair factors (e.g., 53BP1 and RIF1) to DSB regions^{6–8}. During V(D)J recombination, repair of DSBs is mediated by the classical non-homologous end joining (c-NHEJ) pathway to produce a functional V-region exon¹. During CSR, DSBs within two switch regions are repaired primarily by the c-NHEJ machinery and to a lesser degree by the alternative end joining (A-EJ) pathway^{9–11}, leading to a replacement of the μ constant region with another constant region downstream of the recombined V(D)J segment. c-NHEJ involves ligation of DNA ends with little to no homology, whereas A-EJ, which is not well defined, involves regions of microhomology (MH) for end ligation^{11,12}.

Studies have demonstrated that ubiquitination is a critical mechanism in the regulation of signaling transduction in many biological processes, including immune responses¹³, but the functions of deubiquitinases in B cells are not clear. In our previous efforts of searching for new factors that are involved in the CSR process, components of the SAGA (Spt-Ada-Gcn5-acetyltransferase) deubiquitinase complex were identified in a whole-genome RNA interference screen as being required for CSR in the CH12F3-2 (CH12) B-cell line¹⁴. The SAGA complex deubiquitinase Usp22 removes ubiquitin from histone H2B at lysine 120, while addition of this histone mark is catalyzed by the E3 ubiquitin ligase RNF20/RNF40 heterodimer^{15,16}. H2B monoubiquitination at lysine 120 (hereafter referred to as H2Bub) has been implicated in the DNA damage response, as the addition of a ubiquitin moiety to H2B was proposed to induce chromatin relaxation, thereby increasing the accessibility of DNA repair factors to DNA damage^{16,17}. Our previous work with CH12 cells demonstrates that Usp22 is required for CSR in vitro¹⁴. However, as CH12 cells are a lymphoma-derived cell line¹⁸, investigation of Usp22 function in more physiological conditions, such as B-cell development and CSR in vivo, is required.

To assess whether Usp22 is involved in the repair of programmed DSBs in B cells in vivo, we here generate Usp22^{flox/flox} mice and cross these mice with CD19-cre or Mb1-cre to knock out Usp22 specifically in B cells. B-cell-specific Usp22 KO mice have defects in CSR to various Ig isotypes, but not to IgA. IgG CSR is primarily mediated by the c-NHEJ pathway, whereas IgA CSR is more dependent on alternative end joining, indicating that CSR to different isotypes may involve distinct DNA repair pathways. Early pro-B ablation of Usp22 results in the blockade of B-cell development and defects in V to DJ recombination,

supporting other findings that Usp22 promotes c-NHEJ. In summary, by creating the first KO mice of the SAGA complex, we show that Usp22 has an important function in repairing DSBs that occur during B-cell development.

Results

Generation of B-cell-specific Usp22 KO mice. Previous work with the CH12 cell line suggested that Usp22 has a critical role in DSB repair pathways that govern CSR (Fig. 1a). To test whether Usp22 is necessary to repair programmed DSBs that occur during B-cell development in vivo (i.e., V(D)J recombination and CSR), we employed the *Cre-LoxP* system to generate Usp22 conditional KO mice, as Usp22 is essential for mouse embryogenesis¹⁹. Usp22^{flox/flox} mice (Fig. 1b) were crossed with CD19-cre mice²⁰ to knock out Usp22 in pre-B cells. Quantitative PCR (qPCR) analysis showed that Usp22 messenger RNA was reduced in spleen B cells from CD19-cre-Usp22 KO mice compared with wild-type (WT) littermates (Fig. 1c). Lipopolysaccharide (LPS) stimulation resulted in a decrease in Usp22 mRNA level in WT B cells when compared to the unstimulated cells (Supplementary Fig. 1a). Consistent with its role in deubiquitinating H2B, we found that the level of H2Bub was markedly increased in splenic B cells from CD19-cre-Usp22 KO mice (Fig. 1d and Supplementary Fig. 1b). We found that deletion of Usp22 did not markedly affect various spleen B-cell subsets (Fig. 1e and Supplementary Fig. 1c–e).

To evaluate whether B-cell deletion of Usp22 affects CSR in vivo, we first assayed the levels of various Ig isotypes in the serum of Usp22 KO or control mice. We found that the levels of polyclonal IgG1 and IgG3 isotypes were reduced and IgM was increased in the serum of naive CD19-cre-Usp22 KO mice compared with naive WT littermates (Fig. 1f). Interestingly, no defect in the serum IgA level was observed in CD19-cre-Usp22 KO mice (Fig. 1f). As IgA has an essential role in the control of intestinal microbiota²¹, we also tested the level of polyclonal IgA in the feces and also found no defect in fecal IgA levels in CD19-cre-Usp22 KO mice (Fig. 1f). These data demonstrated that Usp22 is critical for H2B deubiquitination in primary B cells and is required for CSR to IgG subclasses but not to IgA, under homeostatic conditions.

Usp22 KO mice exhibited defects in IgG but not IgA responses.

To further evaluate the role of Usp22 on CSR, we first utilized Nitrophenyl Chicken Gamma Globulin (NP-CGG) as a model antigen to immunize mice²². At day 22 post-NP immunization, we found that anti-NP IgG1 levels were reduced, whereas anti-NP IgM levels were increased in CD19-cre Usp22 KO mice, compared with WT littermates (Supplementary Fig. 2a). We observed that the number of NP-specific IgG⁺ antibody secreting cells was reduced in the spleen of Usp22 KO mice, compared with WT littermates (Fig. 2a). To measure antigen-specific IgA responses, mice were infected with rotavirus²³, as IgA is the predominant Ig isotype induced by this pathogen in the small intestine and contributes to fecal rotavirus antigen clearance²⁴. Enzyme-linked immunosorbent assay (ELISA) analysis of fecal anti-rotavirus IgA revealed no defect in the generation of anti-rotavirus IgA in the CD19-cre-Usp22 KO mice compared with WT littermates (Fig. 2b). Furthermore, we found no defect in IgA⁺ rotavirus-specific antibody secreting cells in the lamina propria or bone marrow (BM), or in fecal rotavirus antigen clearance in CD19-cre-Usp22 KO mice compared with WT littermates (Fig. 2c and Supplementary Fig. 2b). Hence, expression of Usp22 by B cells is required to mount antigen-specific IgG responses, but not antigen-specific IgA responses.

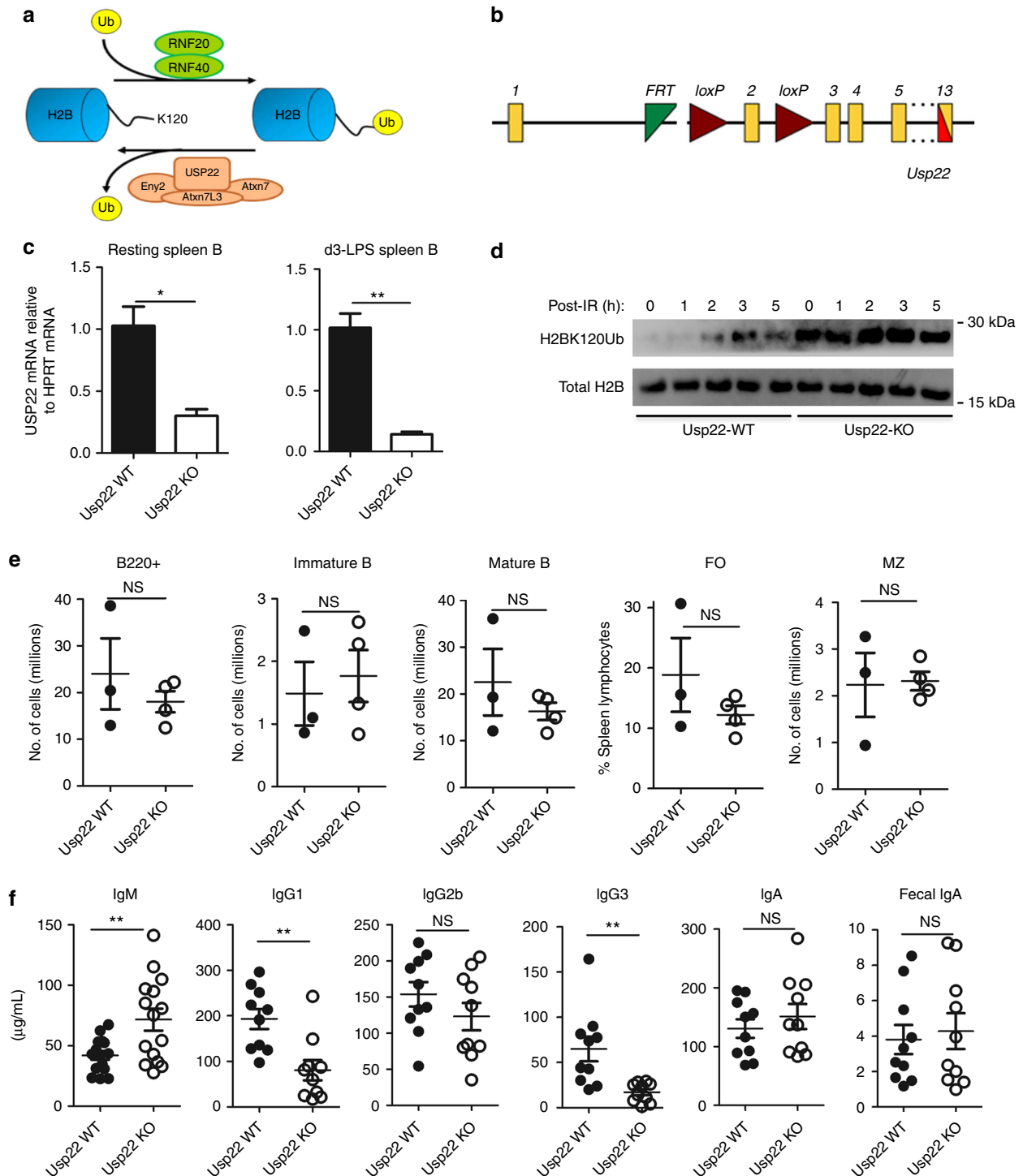


Fig. 1 Spleen B-cell profiles and total Ig isotype analysis of *Usp22* KO or WT mice. **a** Schematic showing the dynamic regulation of histone H2B ubiquitination (Ub). Addition of ubiquitination to H2B is mediated by RNF20/RNF40, while the removal of ubiquitination from H2B is mediated by SAGA complex that is composed of Usp22, Eny2, Atxn7, and Atxn7L3. **b** The structure of targeted *usp22* locus. The protein-encoding exon 2 (133 bp) of the *usp22* gene was flanked by *loxP* sites (triangles). *Usp22^{fllox/fllox}* mice are bred to CD19-cre or Mb1-cre mice to delete exon 2, leading to disruption of *usp22* gene expression specifically in B cells. **c** Spleen B cells were purified from CD19-cre-*Usp22* KO mice or WT littermates. qPCR analysis of *Usp22* mRNA was performed with resting spleen B cells or B cells that were stimulated with LPS for 3 days ex vivo ($n = 3$ mice per group). Data represent two independent experiments. **d** Spleen B cells from CD19-cre-*Usp22* KO and WT littermate mice were stimulated with LPS for 2.5 days, exposed to 8 Grays of γ -radiation, and then collected at various time points for western blot analysis of H2B monoubiquitination (H2BK120Ub). Data represent four independent experiments. **e** Absolute numbers analysis of spleen B cells from CD19-cre-*Usp22* KO and WT littermates. FO, follicular B cells; MZ, marginal zone B cells. Data represent two independent experiments each with three to four mice per group. **f** Serum analysis of various Ig isotypes in unimmunized CD19-cre-*Usp22* KO and WT littermates, as well as fecal IgA from the same mice ($n = 10$ mice per group). Data in **c**, **e**, and **f** were presented as mean \pm SEM and were analyzed using two-tailed unpaired Student's *t*-test. * $p < 0.05$ and ** $p < 0.01$; NS, not significant

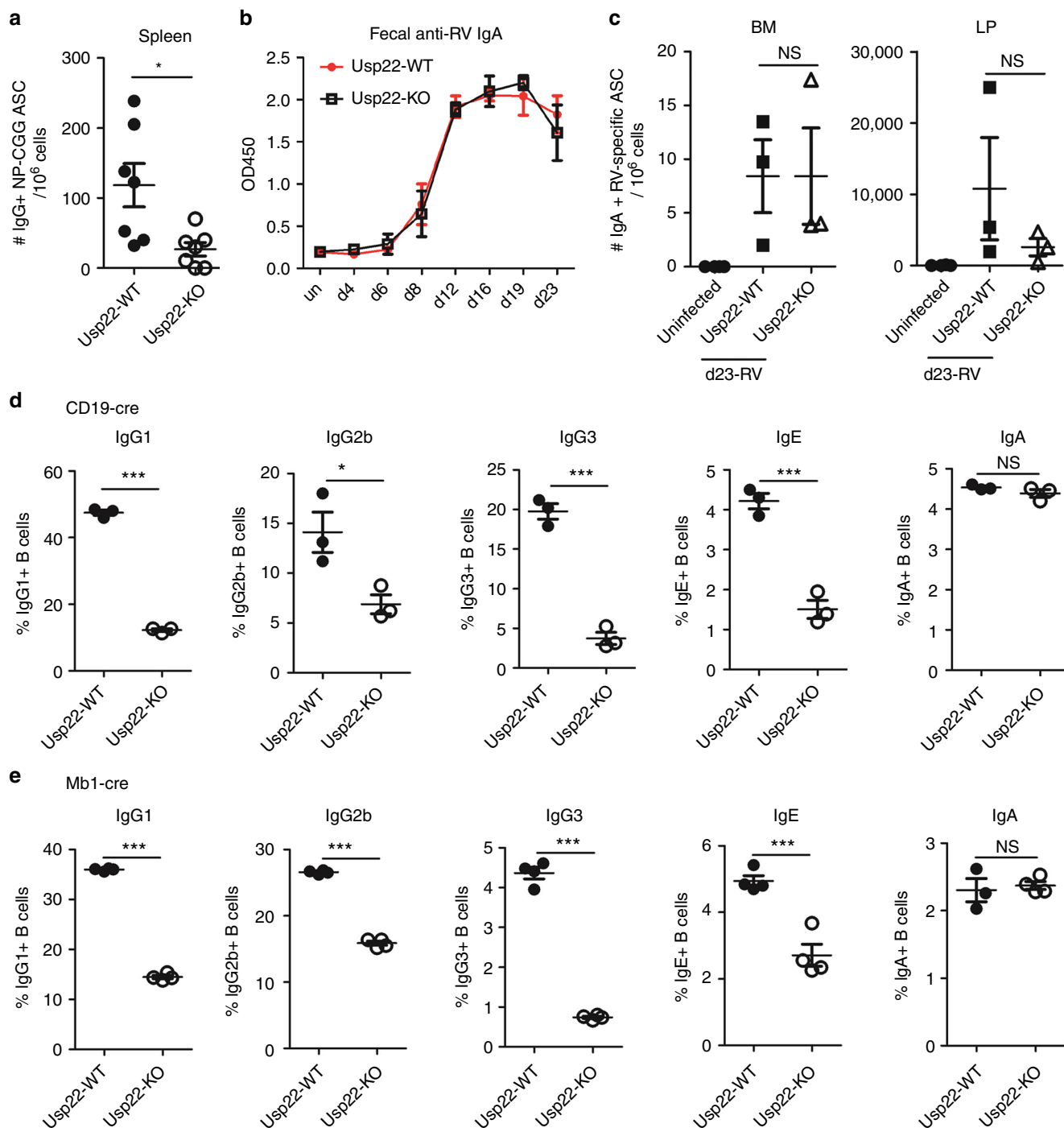


Fig. 2 Usp22 KO mice exhibited defective IgG/IgE CSR but not IgA CSR. **a** NP₂₅-CGG plus alum was intraperitoneally injected into CD19-cre Usp22 KO or WT littermate mice. At d22 post immunization, mice were subjected to NP-specific IgG⁺ ELISPOT assay to measure the amount of NP-specific IgG⁺ antibody secreting cells (ASC) in the spleen ($n = 7$ mice per group). Data were combined from two independent experiments. **b** Rotavirus (RV) was orally administered to CD19-cre-Usp22 KO or WT littermates. Fecal samples were collected at the indicated time-points post-RV infection, followed by fecal supernatant preparation. The 1:2 dilution of fecal supernatant was used for fecal anti-RV IgA ELISA assay. Data was analyzed by two-way ANOVA. **c** ELISPOT assays were performed at d23 post-RV infection, to measure the numbers of IgA⁺ RV-specific antibody secreting cells in lamina propria (LP) and bone marrow (BM), respectively. Data in **b** and **c** represent two independent experiments each with three mice per group. **d** Splenic B cells from CD19-cre-Usp22 KO or WT littermates were ex vivo induced to switch to IgG1, IgG2b, IgG3, IgE, and IgA ($n = 3$ mice per group). **e** Same as **d**, except that Mb1-cre Usp22 KO mice were used ($n = 3-4$ mice per group). Data in **d** and **e** represent three independent experiments; data in **a** and **c-e** were analyzed using two-tailed unpaired Student's *t*-test. Data were presented as mean \pm SEM. * $p < 0.05$ and *** $p < 0.001$; NS, not significant

To determine whether the defect in CSR in Usp22-deficient B cells is cell intrinsic, we induced CSR to various Ig isotypes *ex vivo* using purified spleen B cells. We found that CSR to IgG1, IgG2b, IgG3, and IgE were markedly reduced in spleen B cells from CD19-cre-Usp22 KO mice, compared with littermate controls (Fig. 2d and Supplementary Fig. 2c). Again, surprisingly, IgA CSR was normal in CD19-cre-Usp22 KO splenic B cells (Fig. 2d). To eliminate the possibility that this phenomenon was due to the CD19-cre transgene, we crossed Usp22^{lox/lox} mice with Mb1-cre mice to delete Usp22 in pro-B cells and induced CSR *ex vivo*²⁵. We again observed defects in IgG and IgE CSR, but not in IgA CSR in splenic B cells from Mb1-cre-Usp22 KO mice (Fig. 2e). Collectively, these data suggest that Usp22 is required for switching to IgG and IgE, but not to IgA, in splenic B cells. In addition, we isolated B cells from lymph nodes (LNs) and found that CD19-cre-Usp22 KO LN B cells were also defective in IgG1 CSR *ex vivo* when compared with littermate control (Supplementary Fig. 2d). Interestingly, we observed that Usp22 KO LN B cells exhibited a minor defect in IgA CSR (Supplementary Fig. 2d). The minor difference in IgA CSR between spleen and LN B cells may be due to the possibility that mature B cells are more predominant in LN than in the spleen.

As Mb1-cre-mediated gene deletion can occur in early pro-B cells before V(D)J rearrangement²⁵, we tested whether Usp22 is involved in the repair of DSBs that occur during V(D)J recombination. Hence, we analyzed B-cell profiles in the BM using the “Hardy” staining scheme²⁶. The early B-lineage cells (Hardy Fractions A and B) actively undergo D to J rearrangement (in Fraction B); up to one quarter of these early B cells also undergo V to (D)J recombination in their IgH alleles^{27,28}. We observed that early pro-B cells (B220⁺CD43⁺), especially the Fraction B subset (Fr B: CD43⁺/B220⁺/CD24⁺/BP-1⁻), were markedly increased in the BM of Mb1-cre-Usp22 KO mice, compared with WT littermates (Supplementary Fig. 3a-c), indicative of a blockade in B-cell development in Usp22 KO mice. We evaluated V(D)J recombination at the molecular level and found that distal V_H to DJ_H segment recombination, but not proximal V_H-to-DJ_H or D-to-J recombination, seemed to be impaired in pro-B cells from Mb1-cre-Usp22 KO mice (Supplementary Fig. 3d-e). These data suggest that Usp22 is involved in the long-range V(D)J recombination and B-cell development.

Impaired γ H2AX levels in Usp22 KO spleen B cells. To investigate the potential mechanisms for IgG/IgE CSR defects in Usp22-deficient B cells, we first assessed whether AID expression was impaired, as AID is essential for CSR⁴. We found that AID was increased at both mRNA and protein levels in spleen B cells from CD19-cre-Usp22 KO mice compared with WT littermates (Fig. 3a and Supplementary Fig. 4a), which might be due to the role of Usp22 in regulating the gene transcription²⁹. However, these data are inconsistent with a reduction in CSR to IgG/IgE in Usp22-deficient B cells. One possibility that could explain the CSR defect to IgG/IgE, but not IgA in Usp22-deficient B cells, is the reduction of germline transcripts in γ , ϵ switch regions, but not α switch region. By evaluating the germline transcripts at day 2 post-CSR stimulation, we found comparable levels of μ , γ 1, and α germline transcripts between Usp22 KO and WT splenic B cells (Supplementary Fig. 4b-c). To test whether AID function at the μ and γ 1 switch region was affected, we sequenced the regions upstream of the μ and γ 1 switch region, respectively. However, we found no significant difference in AID mutation frequency in splenic B cells between CD19-cre-Usp22 KO and WT group (Table 1), which is consistent with our previous studies with Usp22 KO CH12 cells¹⁴. Together, these data indicate that differential effects of Usp22 deficiency on IgG/IgE vs IgA CSR in

primary B cells are independent of AID activity, suggesting that repair of DSBs downstream of AID is different when leading to IgG/IgE CSR than IgA.

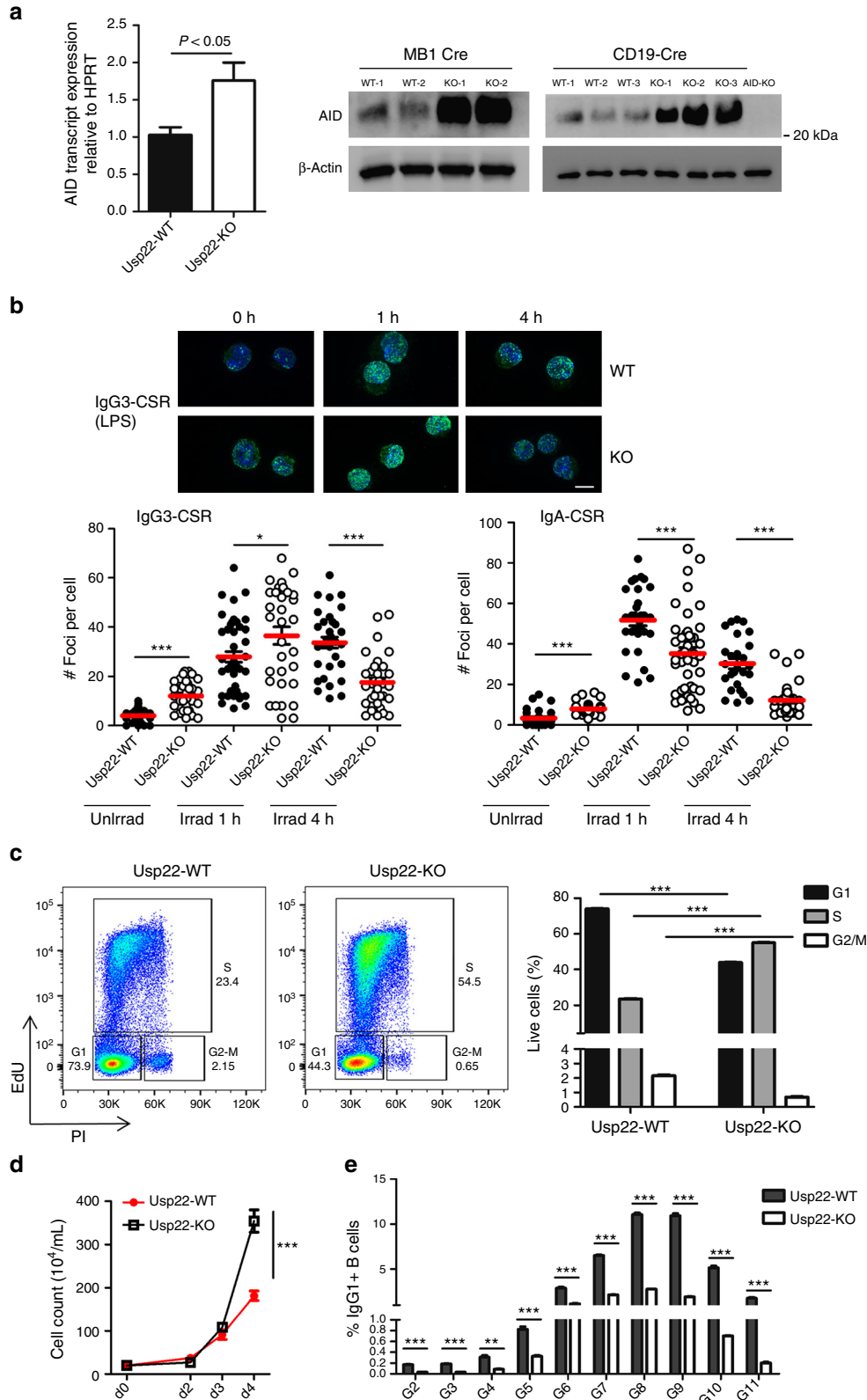
γ H2AX has a critical role in DSB repair by recruiting various DNA repair factors to DSB regions⁶⁻⁸, and it has been shown that premature degradation of γ H2AX signaling leads to impaired DNA damage repair³⁰. To test whether enhanced H2Bub has an impact on γ H2AX kinetics in mice, splenic B cells were stimulated with LPS and then exposed to γ -radiation, followed by γ H2AX immunofluorescent staining. We found that γ H2AX kinetics were altered in CD19-cre-Usp22 KO B cells, with a marked decrease in γ H2AX four hours post irradiation (Fig. 3b). We also observed a premature degradation of γ H2AX in Usp22 KO group under conditions that lead to IgA CSR (Fig. 3b), which is consistent with our previous data in IgA-switched CH12 cells¹⁴. As a defect in γ H2AX signaling could manifest in a defect in DSB repair that can impair cell cycle progression during CSR, we evaluated whether the cell cycle was altered in Usp22 KO primary B cells. By pulsing cells with Edu and then staining with propidium iodide (PI), we found that LPS-stimulated spleen B cells from CD19-cre-Usp22 KO mice exhibited an increased proportion of S-phase cells and a decreased proportion of G1 and G2-M phases compared with controls (Fig. 3c and Supplementary Fig. 4d). Consistent with this finding, proliferation assays showed that LPS-stimulated Usp22-KO B cells proliferated more quickly than WT B cells (Fig. 3d). However, the IgG/IgE CSR defects in Usp22-deficient spleen B cells are unlikely due to alterations in cell cycle, as CSR to IgG1 is defective in CD19-cre-Usp22 KO B cells at various stages of division (Fig. 3e and Supplementary Fig. 4e). Collectively, these data show that Usp22 deficiency results in premature degradation of γ H2AX signaling and a potentially disrupted G₁-S checkpoint, which may manifest in impaired DNA repair during CSR.

IgA CSR is more dependent on A-EJ than IgG CSR. As V(D)J recombination requires c-NHEJ³¹, the impaired pro-B-cell development in Mb1-cre-Usp22 KO mice suggests that Usp22 is critical for c-NHEJ. The repair of DSBs during CSR is mediated by both the c-NHEJ pathway and A-EJ pathway^{9,10}. Unlike DSBs repaired by A-EJ, DSBs repaired by c-NHEJ typically have little to no MH between the donor and acceptor switch regions¹¹. As Usp22 KO splenic B cells exhibited defective CSR to IgG and IgE but not IgA, we hypothesized that CSR to various Ig isotypes may rely on different DNA repair pathways to various degrees. To test this hypothesis, we examined switch junctions from IgG1- vs IgA-switched spleen B cells, as analysis of MH usage at switch junctions can reflect the DNA repair pathways that were utilized during CSR. Sequencing of IgG1-switched spleen B cells revealed that the MH length between the μ and γ 1 switch regions is comparable between CD19-cre-Usp22 KO and WT littermates (MH: 2.4 vs 2.2, $P = 0.75$) (Fig. 4a), although a trend of increased 6 + bp MH usage was observed in Usp22-KO IgG1 B cells (9%) when compared with Usp22-WT B cells (2%). In contrast, we found a significantly longer MH between the μ and α switch regions in IgA-switched CD19-cre-Usp22 KO spleen B cells, compared with WT littermates (MH: 3.0 vs 1.9, $P < 0.05$) (Fig. 4b). The percentage of insertions was slightly decreased in Usp22 KO B cells when compared with WT control (Fig. 4a,b). The pattern of breakpoint locations, which were distributed across the switch regions, were comparable between Usp22-WT and -KO groups (Fig. 4c,d).

The increased MH usage in μ - α switch regions but not μ - γ 1 switch regions in Usp22-deficient B cells has been observed before in DNA Ligase IV- and DNA-PKcs-deficient human B cells (i.e., defective in c-NHEJ)^{32,33}, and suggests that CSR to IgA

employs A-EJ more efficiently when c-NHEJ is impaired, while CSR to IgG1 does not. These results further suggest that Usp22 promotes the c-NHEJ but not the A-EJ pathway. To further validate the distinct dependence of IgG and IgA CSR on c-NHEJ vs A-EJ, we evaluated the surface Ig isotype in spleen B cells from

53BP1-deficient mice, which are deficient in c-NHEJ³⁴, after ex vivo CSR stimulation. We found that 53BP1^{-/-} B cells exhibited a less severe defect in IgA CSR (~60% reduction, compared with controls) than CSR to other Ig isotypes (~80–90% reduction) (Fig. 5a). In addition, we used the SUV4-20 inhibitor



A-196 (A-197 as the control compound) to suppress c-NHEJ during ex vivo CSR of WT spleen B cells³⁵. Inhibition of c-NHEJ caused a defect in IgG1 CSR (~50% reduction), but not IgA CSR (Fig. 5b).

To determine why CSR to IgA is more dependent on the A-EJ pathway than switching to other isotypes, we analyzed the sequence homology between switch regions within the mouse IgH locus. We reasoned that since A-EJ utilizes microhomologies during the reaction, recombining sequences with increased homology might favor A-EJ over c-NHEJ. We found that in both C57BL/6 and BALB/c mice, a higher degree of homology was observed between S μ and S α , when compared with that between S μ and S γ 1, S γ 2b, and S γ 3 switch regions (Fig. 5c,d and Supplementary Fig. 5-6). It is notable that S μ and S ϵ switch regions also had a relatively high degree of nucleotide identity, although to a lesser degree as compared with the S μ and S α switch regions. Hence, the high degree of primary DNA sequence identity between S μ and S α switch regions might explain why A-EJ is more efficient during IgA CSR at the molecular level.

Discussion

By generating the first KO mouse of the SAGA complex, we identified Usp22 as a new factor that is essential to repair programmed DNA breaks that occur during B-cell ontogeny. We demonstrate that Usp22 promotes c-NHEJ and CSR in vivo. Interestingly, B-cell-specific ablation of Usp22 resulted in defective CSR to various IgG/IgE isotypes but not to IgA. We further demonstrated that CSR to IgG/IgE is primarily mediated by c-NHEJ, whereas CSR to IgA is more dependent on MH-mediated A-EJ. Indeed, consistent with a previous report that measured serum Ig isotypes in 53BP1^{-/-} mice³⁶, we found by measuring surface Ig isotypes that 53BP1^{-/-} B cells exhibited a less severe defect in IgA CSR than CSR to other Ig isotypes. In addition, we observed that chemical inhibition of c-NHEJ has strong effects on IgG CSR but not IgA CSR, which is similar to the CSR phenotype in Usp22-deficient B cells. The difference in IgA CSR between Usp22 KO mice and 53BP1^{-/-} mice may be due to the fact that c-NHEJ is essentially null in 53BP1^{-/-} mice but is likely only reduced in Usp22 KO mice. In addition to IgA CSR, it has been reported that A-EJ pathways are also preferentially utilized for CSR to IgD^{37,38}. As μ and α switch regions from both human and mice share higher sequence identity compared with other switch regions, this might be the reason for the increased dependence of A-EJ for IgA CSR, which in turn would suggest that primary DNA sequences can partly dictate the usage of DNA repair pathways.

Ubiquitination-mediated signaling transduction has important roles in many biological processes, including various aspects of immune functions¹³. In contrast to ubiquitylating enzymes, the roles of deubiquitinases are less well studied, especially in the

context of B cells. Histone H2B has been implicated in DNA damage response, as H2Bub at lysine 120 is thought to induce changes in chromatin conformation, making damaged DNA accessible by various repair factors^{16,17}. Usp22 has been shown to deubiquitinate both histone H2A and H2B in biochemical assays^{39,40}. A recent report showed that H2Bub levels are not increased in Usp22-deficient HEK293T cells due to redundancy with other deubiquitinases⁴¹. However, we found that Usp22 deletion in primary spleen B cells resulted in a marked increase in H2Bub, which is consistent with our findings in Usp22-KO CH12 cells¹⁴, indicating that Usp22 is essential for H2B deubiquitination in B cells, and that other deubiquitinases have significant backup roles to Usp22 in these cells.

V(D)J recombination is essential for the surface expression of BCR and T-cell receptor¹. We found that Usp22 deletion in early B cells mediated by Mb1-cre caused a block at the Fraction B stage during B-lymphopoiesis. At the molecular level, we observed that long-range V-(D)J rearrangement seems to be impaired in the Mb1-cre-Usp22 KO mice, which is similar to the defective V-(D)J recombination phenotype observed in Pax5-, IL-7R-, or 53BP1-deficient mice^{27,42-44}, or patients with NIPBL mutations⁴⁵. Nevertheless, more work needs to be carried out to establish a role for Usp22 in V(D)J recombination, and whether the defect in B cell development is due to altered cell cycle and/or cell death in the Usp22 KO mice. It also remains to be investigated why distal vs proximal V-to-DJ recombination has different requirements for certain c-NHEJ factors, such as 53BP1 and Usp22.

Phosphorylation of H2AX has a critical role in the DNA damage response by recruiting various DNA repair factors to damage regions⁶⁻⁸, and it has been shown that premature degradation of γ H2AX signaling impairs DNA repair³⁰. We found that ablation of Usp22 in B cells resulted in a defect in irradiation-induced γ H2AX levels at later time-points (i.e., 4 h post irradiation)¹⁴. The potential mechanisms by which excessive H2Bub affects γ H2AX signaling are unknown. It is possible that excessive H2Bub inhibits the recruitment/stability of γ H2AX kinase (i.e., ATM and DNAPK) via steric hindrance and/or preferentially recruits certain γ H2AX phosphatases to sites of DNA damage.

IgA is the most abundant antibody isotype in the body and has an essential role in the control of pathogen invasion and commensal bacteria at mucosal surfaces, such as the gastrointestinal tract⁴⁶. Many recent studies including our own have demonstrated that dysregulation of the microbiome are linked to many diseases, such as inflammatory bowel disease, neurologic diseases, and various cancers^{47,48}. In our previous report, we found that knockdown or KO of Usp22 caused a defect in IgA CSR in the CH12 cell lines¹⁴. Here, by generating B-cell-specific Usp22 KO mice, we found that Usp22 ablation led to defects in CSR to

Fig. 3 Impaired γ H2AX levels in spleen B cells from CD19-cre-Usp22 KO mice. **a** AID mRNA measured by qPCR of d3-LPS stimulated spleen B cells from CD19-cre-Usp22 KO or WT littermates (left panel; $n = 5$ mice per group). AID blot analysis of d3-LPS stimulated spleen B cells from Mb1-cre or CD19-cre Usp22 KO or their WT littermates (right panel; $n = 2-3$ mice per group); AID-KO cells were used as control and data represent two or three independent experiments. **b** Spleen B cells from CD19-cre-Usp22 KO and WT littermates were stimulated for IgG3 CSR (by LPS) or for IgA CSR (by LPS+ IL-4+ TGF- β + IL-5+ anti-IgD dextran) for 2.5 days, exposed to γ -radiation, and then collected for γ H2AX immunofluorescent staining. Line within micrograph represents 10 μ m. The number of γ H2AX foci per cell was analyzed 1 or 4 h post irradiation for Usp22-WT (black circles) and CD19-cre-Usp22-KO (white circles) (bottom panel), and representative images for IgG3-CSR group (γ H2AX in green and DAPI in blue) are shown in the top panel. Approximately 30-50 cells were analyzed per sample and data represent two or three independent experiments. **c** Representative flow cytometry plots (left panel) and compiled cell cycle analysis (right panel) of Usp22-WT and CD19-cre-Usp22-KO spleen B cells. Cells were stimulated with LPS for 2.5 days and then incubated with EdU for 4 h, before FACS staining ($n = 3$ samples per group). **d** Purified splenic B cells from CD19-cre Usp22-KO or WT littermates was stimulated with LPS and growth of these cells was monitored over time ($n = 3$ samples per group). Data were tested by two-way ANOVA. **e** CFSE-pulsed spleen B cells from CD19-cre-Usp22 KO or WT littermates were stimulated by LPS plus IL-4 for CSR to IgG1 for 4 days. The gating (G2 to G11) is based on the intensity of CFSE and the percentage of IgG1 switch per gate is summarized ($n = 3$ samples per group). Data in **c-e** represent two independent experiments; data in **a-c** and **e** were analyzed using two-tailed unpaired Student's *t*-test. Data were presented as mean \pm SEM. * $p < 0.05$, ** $p < 0.01$, and *** $p < 0.001$

Table 1 Frequency of mutations upstream of switch μ or $\gamma 1$ regions

	Usp22 WT		Usp22 KO	
	S' μ ^c	S' $\gamma 1$ ^d	S' μ ^c	S' $\gamma 1$ ^d
Sequences (#)	54	47	50	35
Nucleotides sequenced (#)	30,742	24,974	26,404	17,562
Mutations (#)	14	5	16	3
Mutation frequency ^a	4.55×10^{-4}	2.00×10^{-4}	6.05×10^{-4}	1.71×10^{-4}
Mutations at G/C (%)	86	100	100	100
AID hotspot mutations (%) ^b	79	100	88	100
Deletions/insertions (#)	0	0	0	1

^aFrequency is defined as unique mutations/nucleotide sequenced. ^bMutations at WRC and GYW motifs, where W = A/T, R = A/G, and Y = T/C. ^cCells stimulated to IgA ($n = 4$ mice per group). ^dCells stimulated to IgG1 ($n = 3$ mice per group).

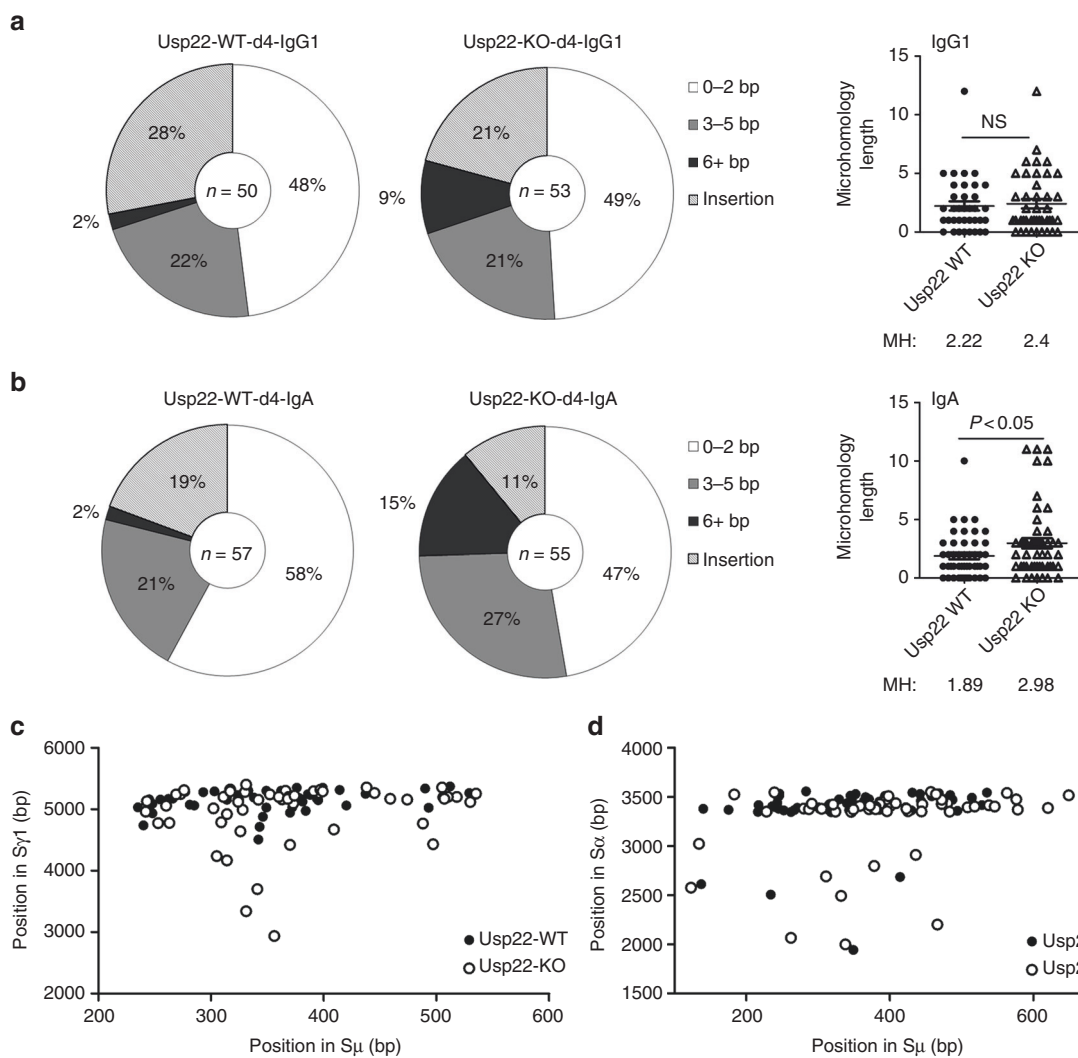


Fig. 4 Microhomology analysis of switch junctions of IgG1- or IgA-switched spleen B cells. Spleen B cells isolated from CD19-cre-Usp22 KO or WT littermates were induced for IgG1 (**a** and **c**) or IgA (**b** and **d**) CSR ex vivo for 4 days. IgG1 and IgA switch junctions were cloned from these cells, and subjected to sequencing. Approximately 50–60 unique switch junction sequences were analyzed per group. **a** S μ /S $\gamma 1$ or **b** S μ /S α junctions were categorized based on their microhomology usage: near-blunt joins (0–2 bp), joins with microhomology (3–5 bp or 6 + bp), or insertions. The microhomology length (MH) used by each unique switch junction sequence are summarized (right panel). **c** Distribution of breakpoints across μ or $\gamma 1$ switch regions for IgG1-switched Usp22-WT or -KO cells. **d** Distribution of breakpoints across μ or α switch regions for IgA-switched Usp22-WT or -KO cells. Data in **a–d** were combined from three mice per group; data in **a** and **b** were presented as mean \pm SEM and were analyzed using two-tailed unpaired Student's *t*-test. NS, not significant

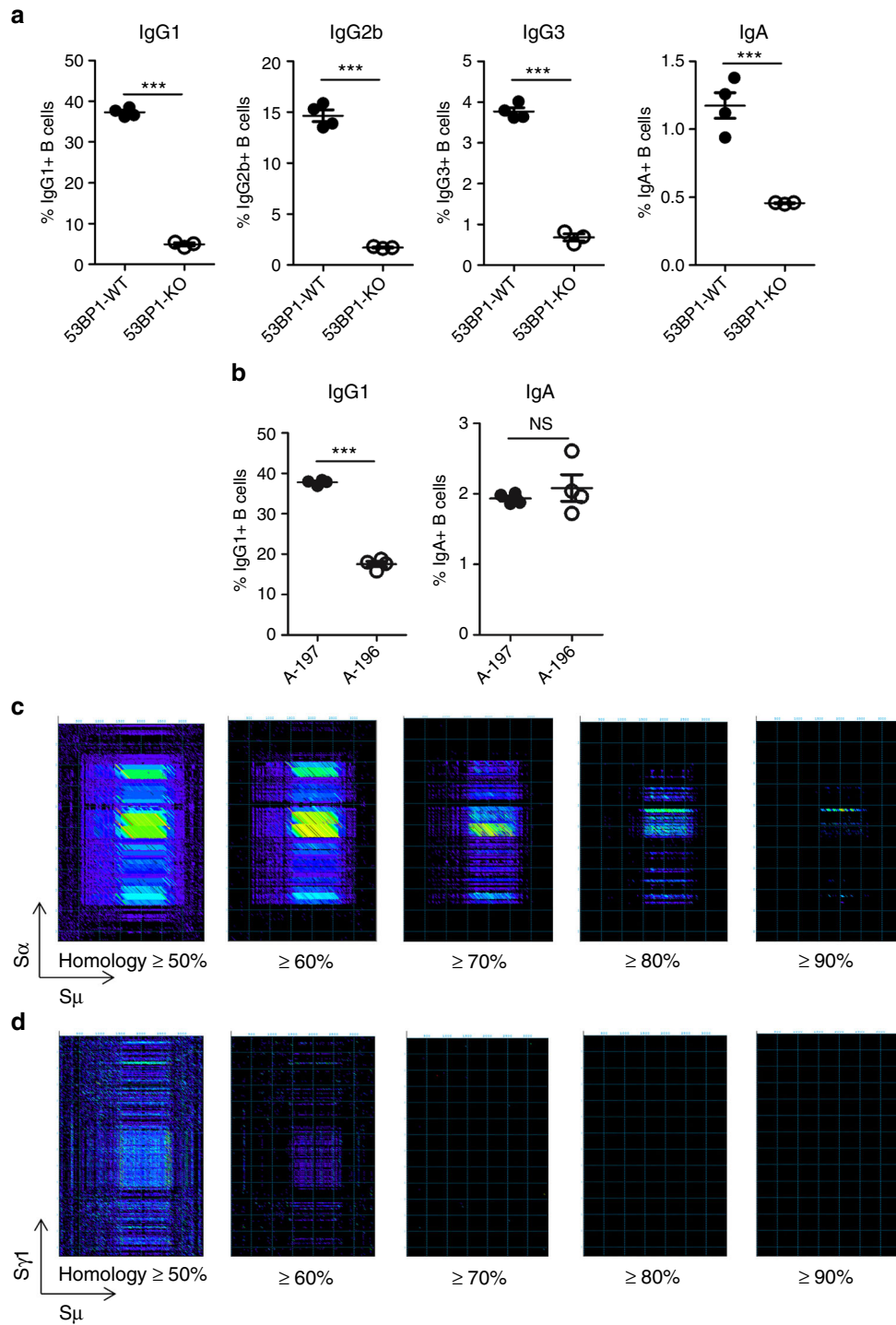


Fig. 5 IgG1 CSR primarily relies on c-NHEJ, whereas IgA CSR is more dependent on A-EJ. **a** Spleen B cells isolated from 53BP1 KO or WT littermates were induced for ex vivo IgG1, IgG2b, IgG3, or IgA CSR for 4 days. 53BP1^{-/-} B cells (deficient in c-NHEJ) exhibited a less severe defect in IgA CSR (~60% reduction) compared with IgG CSR (~80–90% reduction). Data represent two independent experiments each with three to four mice per group. **b** A-196 (10 μM) was used to inhibit c-NHEJ during the ex vivo CSR of WT spleen B cells and A-197 is the control compound. Inhibition of c-NHEJ markedly reduced IgG1 CSR, but not IgA CSR (*n* = 4 samples per group). Data represent three independent experiments. **c, d** The switch region sequence of S_μ on the IgH locus of C57BL/6 background mice were compared with that of **c** S_α or **d** S_{γ1}. Dot Matrix analysis of the mouse switch regions. The dots represent homologies between two switch regions with a search length of 30 bp and defined percentage of identity. Data in **a** and **b** were presented as mean ± SEM and were analyzed using two-tailed unpaired Student's *t*-test. ****p* < 0.001; NS, not significant

various Ig isotypes except IgA in vivo. The ex vivo CSR assays revealed that Usp22 KO splenic B cells are defective in almost all the isotypes, except IgA. However, Usp22 KO LN B cells are defective in both IgG1 and, to a lesser extent, IgA CSR, which is similar to the CSR phenotype with *53BP1*^{-/-} mice. The discrepancy between these two studies is unclear. It is notable that CH12 B-cells have a B1 B-cell phenotype, whereas the vast majority of splenic B cells have a B2 B-cell phenotype^{49,50}, and recent studies have reported major differences between B1 and B2-B cells regarding their CSR toward IgA^{50–52}. Nevertheless, as Usp22 deletion in vivo caused strong defects in various Ig isotypes but less so to IgA, Usp22 could be exploited as a therapeutic target in IgG or IgE-mediated autoimmune diseases, such as systemic lupus erythematosus, autoimmune thrombocytopenia, and asthma. It is expected that Usp22 inhibitors have the potential of ameliorating the pathogenesis of these antibody-mediated autoimmune diseases, without disturbing the homeostasis of the gut microbiota. Furthermore, our findings, that IgA CSR can utilize two DNA repair pathways while IgG CSR only employs one, highlight the biological need for IgA production as observed in μ MT mice, which can produce IgA but not other isotypes⁵³.

In summary, we report that Usp22 is the first deubiquitinase that regulates both V(D)J recombination and CSR in vivo by promoting c-NHEJ. We found that IgG CSR is primarily mediated by c-NHEJ, while IgA CSR is more dependent on A-EJ, indicating that CSR to different isotypes involve distinct DNA repair pathways.

Methods

Mice. C57BL/6 WT mice (Charles River Laboratory, St. Constant, QC, Canada; 6–8-week-old females) were bred in our Animal Vivarium facility at the University of Toronto. Mice containing two *FRT* sites in the upstream of exon 2 of Usp22 and two *loxP* sites flanking exon 2 of Usp22 were purchased from UC DAVIS KOMP Repository (Davis, CA) and bred with FLP-o deleter mice (The Jackson Laboratory), to generate Usp22^{fllox/+} mice. Usp22^{fllox/+} mice were then bred with CD19-Cre (The Jackson Laboratory) or Mb1-Cre mice, respectively. CD19-cre Usp22^{fllox/fllox} mice were bred with Usp22^{fllox/fllox} mice, to generate Usp22 KO (CD19-cre Usp22^{fllox/fllox}) and WT littermates (i.e., Usp22^{fllox/fllox}) for experimental use (sex-matched; 12–16 weeks old). Mb1-cre Usp22^{fllox/+} mice were bred with Usp22^{fllox/fllox} mice, to generate Mb1-cre Usp22^{fllox/fllox} (KO), Mb1-cre Usp22^{fllox/+} (het), and WT littermates (i.e., Usp22^{fllox/fllox} or Usp22^{fllox/+}) for experimental use (sex-matched; 6–7 weeks old). *53BP1*^{+/-} mice were bred with *53BP1*^{+/-}, to generate *53BP1*^{-/-} and WT littermates for experimental use (sex-matched; ~8 weeks old). All the mice were maintained under pathogen-free conditions. The experimental procedures were approved by the Animal Care Committee of University of Toronto.

Usp22 and AID qPCR. Spleen B cells were purified from CD19-cre Usp22 KO or WT littermates (around 12–16 weeks old), using the EasySep Mouse B-cell Isolation Kit (Stemcell Technologies). For LPS-stimulated group, spleen B cells (0.2×10^6 /mL) were cultured in the complete RPMI with 50 μ g/mL LPS (Sigma Aldrich) for 3 days. RNA from resting or LPS-stimulated spleen B cells was extracted using TRIzol (Invitrogen) and then treated by DNaseI. The complementary DNA was prepared with the use of a SuperScript III reverse transcription kit (Life Technologies) and subjected to qPCR reactions of Usp22 or AID, with hypoxanthine guanine phosphoribosyl transferase (HPRT) as internal control. The sequences of the qPCR primers are described in the Supplementary Table 1.

AID and H2Bub western blotting. Purified spleen B cells were stimulated with 50 μ g/mL LPS for 3 days and then collected for western blotting with mouse anti-AID monoclonal antibody (Cell Signaling Technology, clone: L7E7, catalog number: 4975; 1/1000 dilution) or rabbit polyclonal anti- β actin antibody (Sigma, catalog number: A2066; 1/1000 dilution). For H2Bub western blotting, the purified spleen B cells were first stimulated with LPS for 2.5 days, exposed to 8 Grays of γ -radiation, and then collected at various time points for western blotting with mouse monoclonal antibody against H2BK120Ub (Millipore, clone: 56, catalog number: 05-1312; 1/1000 dilution), or rabbit polyclonal antibody against total H2B (Abcam, catalog number: ab18977; 1/1000 dilution).

Spleen and BM B-cell profiling. Single-cell suspension of spleen was prepared from CD19-cre-Usp22 KO or WT littermate mice (around 12–16 weeks old), whereas BM cells were extracted from hind legs of Mb1-cre-Usp22 KO or WT

littermates (around 6–7 weeks old), followed by red blood cell lysis. The cells were strained and resuspended in fluorescence-activated cell sorting (FACS) buffer (2% fetal bovine serum in phosphate-buffered saline (PBS)), and incubated with mouse Fc blocker (2.4G2 mAb; 1/100 dilution). As previously described⁵⁴, splenic cells were stained with rat allophycocyanin (APC)-conjugated anti-CD45R/B220 (RA3-6B2; SouthernBiotech; 1/150 dilution), rat eFluor 450-conjugated IgM (II/41; eBioscience; 1/150 dilution), rat phycoerythrin (PE)-conjugated CD93 (AA4.1; eBioscience; 1/50 dilution), and rat fluorescein isothiocyanate (FITC)-conjugated CD23 (B3B4; eBioscience; 1/100 dilution); BM cells were stained with APC-conjugated anti-CD45R/B220, eFluor 450-conjugated IgM, rat PE Cy7-conjugated CD43 (S7; BD Pharmingen; 1/150 dilution), rat FITC-conjugated CD24 (30-F1; eBioscience; 1/100 dilution), and rat PE-conjugated BP-1 (6C3; BioLegend; 1/33 dilution). The stained cells were incubated with PI, acquired on a BD LSRFortessa X-20 flow cytometer (BD Biosciences), and analyzed by FlowJo software (Treestar Inc.).

Total Ig ELISA assay. Sera or fecal pellets were collected from CD19-cre Usp22 KO or WT littermate mice (around 7–8 weeks old), and fecal supernatant was prepared (10% wt/vol) with PBS. The Ig isotype-specific ELISA assays were performed as previously described⁵⁵. Briefly, 96-well ELISA plates (NUNC) were coated with goat antibodies against mouse IgM (catalog number: 1021-01; 1/1000 dilution), IgG1 (catalog number: 1071-01; 1/1000 dilution), IgG2b (catalog number: 1090-01; 1/1000 dilution), IgG3 (catalog number: 1101-01; 1/333 dilution), or IgA (catalog number: 1040-01; 1/500 dilution) (all from SouthernBiotech), respectively, overnight at 4 °C. After blocking with 3% bovine serum albumin (BSA), 1/50-diluted sera or 1/5-diluted fecal samples were added into the wells, followed by serial fourfold dilution. The bound antibodies from sera or fecal supernatant were detected by the appropriate isotype-specific goat anti-mouse Ig that was conjugated with alkaline phosphatase (AP), IgM-AP (catalog number: 1021-04; 1/2000 dilution); IgG1-AP (catalog number: 1070-04; 1/2000 dilution); IgG2b-AP (catalog number: 1090-04; 1/2000 dilution); IgG3-AP (catalog number: 1100-04; 1/4000 dilution); IgA-AP (catalog number: 1040-04; 1/2000 dilution) (all from SouthernBiotech), followed by the development with SIGMAFAST p-Nitrophenyl phosphate substrate.

Ex vivo CSR. Spleen B cells were purified from CD19-cre Usp22 KO (around 12–16 weeks old), Mb1-cre Usp22 KO (around 6–7 weeks old), *53BP1*^{-/-} (around 6–10 weeks old) or their age-matched littermate control mice, using the EasySep Mouse B-cell Isolation Kit. To purify LN B cells, single-cell suspensions of peripheral LNs (inguinal, cervical, and axillary LN) and mesenteric LNs were stained with mouse BV605-conjugated anti-B220 antibody (RA3-6B2; BioLegend; 1/200 dilution), and the sorting was performed with FACS Aria IIu cell sorter (BD Biosciences). Splenic or LN B cells (0.2×10^6 /mL) were cultured in complete RPMI with 50 μ g/mL LPS for 4 days. For IgG1/IgE switching, 25 ng/mL of interleukin (IL)-4 (R&D Systems) was added; for IgG2b switching, 30 μ g/mL dextran-sulfate (Sigma Aldrich) was added; for IgG3 switching, 3 or 10 ng/mL anti-IgD dextran (depending on the lots; Fina BioSolutions LLC) was added; for IgA switching, IL-4 (10 ng/mL), transforming growth factor (TGF)- β (2 ng/mL; R&D Systems), IL-5 (1.5 ng/mL; BD Pharmingen), and anti-IgD dextran (3 or 10 ng/mL; depending on the lots) were added. We noted that the variations in IgG3 or IgA CSR between different batches of experiments are mainly due to the various activities of different lots of anti-IgD dextran. For FACS analysis, cells were surface stained with PE rat anti-mouse IgG1 (A85-1, BD Pharmingen; 1/133 dilution), PE goat anti-mouse IgG2b (SouthernBiotech, catalog number: 1090-09; 1/133 dilution), PE goat anti-mouse IgA (SouthernBiotech, catalog number: 1040-09; 1/133 dilution), and FITC rat anti-mouse IgG3 (R40-82, BD Pharmingen; 1/100 dilution), whereas FITC rat anti-mouse IgE (R35-72, BD Pharmingen; 1/100 dilution) was intracellularly stained⁵⁶. The stained cells were acquired on a FACSCalibur flow cytometer (BD Biosciences) and analyzed by FlowJo software.

For A-196 inhibition assay, splenic B cells were isolated from WT mice (around 6–10 weeks old) and cultured in complete RPMI media with the inhibitor, as previously described⁵⁵. Spleen B cells (0.2×10^6 /mL) were first stimulated with LPS (25 μ g/mL) in the presence of 10 μ M A-196 or control compound A-197 for 1 day. For IgG1 CSR, the cells were changed with new media containing LPS (50 μ g/mL) plus IL-4, and fresh A-196 or A-197 for 4 days. For IgA CSR, splenic B cells were stimulated with LPS (50 μ g/mL), IL-4, TGF- β , IL-5, and anti-IgD dextran for 4 days.

NP-specific ELISA and ELISPOT assay. CD19-cre Usp22 KO or WT littermates (around 12–16 weeks old) were intraperitoneally immunized with 100 μ g NP-CGG (Biosearch Technologies) in alum adjuvant (Thermo Scientific), as we previously described²². At day 22 post immunization, mice were bled for sera and killed for spleen collection. Sera from non-immunized or NP-immunized mice were added to ELISA plates that were coated with NP4-BSA (Biosearch Technologies; binds to high-affinity anti-NP antibodies) or NP32-BSA (Biosearch Technologies; binds to both high-affinity and low-affinity anti-NP antibodies), respectively, as we previously described²². Single-cell suspension of the spleen was prepared and subjected to NP-specific enzyme-linked immunosorbent assay spot (ELISPOT), in

which MultiScreen-HTS-HA filter plates were coated with NP32-BSA. Later steps were performed as previously described²².

Rotavirus-specific ELISA and ELISPOT assay. CD19-cre Usp22 KO or WT littermates (around 12–16 weeks old) were infected with rotavirus as we previously described²³. Fecal pellets were collected from each mouse one day before rotavirus challenge and on the indicated days post infection. Fecal supernatant was prepared (10% wt/vol) with PBS and ½ dilution was used for fecal anti-rotavirus IgA and rotavirus antigen ELISA assays, as previously described²³. At day 23 post rotavirus infection, rotavirus-specific IgA⁺ ELISPOT assay was performed to measure the numbers of IgA⁺ RV-specific antibody-secreting cells from the BM and the lamina propria from the small intestine. Lymphocytes from the lamina propria were prepared by Percol gradient as we previously described²³. BM cells were flushed out from the femurs and tibia of CD19-cre Usp22 KO or WT littermates, followed by red blood cell lysis. MultiScreen-HTS-HA filter plates were coated overnight with inactive rotavirus antigen (Microbox) and then blocked with complete RPMI media. The plates were incubated with twofold serial dilutions of BM cells or lymphocytes from lamina propria overnight, followed by detection with horseradish peroxidase (HRP)-conjugated goat anti-mouse-IgA Ab (SouthernBiotech, catalog number: 1040-05; 1/500 dilution). Then the colorimetric precipitating substrate for HRP, AEC (Vector Laboratories), was used to develop the plate. Positive dots on the membrane within wells were counted with a Nikon stereomicroscope.

V(D)J and D-J PCR. BM cells from Mb1-cre-Usp22 KO or control WT mice (around 6–7 weeks old) were stained with APC-conjugated anti-CD45R/B220, PE Cy7-conjugated CD43, FITC-conjugated CD24, and PE-conjugated BP-1 and PI. The sorting of Hardy Fraction B or C Pro-B cells were performed on a BD Influx Cell Sorter (BD Biosciences), followed by genomic DNA extraction using the proteinase K method. For the distal and proximal V(D)J PCR, genomic DNA from Fraction C of BM B cells was used and two rounds of PCR amplification were performed as previously described²⁸; the first round of PCR reaction, containing both V_HJ588 and V_H7183, and the J_H4E primer, was performed over 30 cycles (1 min at 95 °C, 1 min at 60 °C, and 1.5 min at 72 °C); for the second round of PCR, 1 µl aliquots of the first round PCR reaction was used, containing either V_HJ588 or V_H7183, with the nested J_H4A primer (30 cycles: 1 min at 95 °C, 1 min at 63 °C, and 1.5 min at 72 °C). Glycerinaldehyde 3-phosphate dehydrogenase (GAPDH) was used as loading control, with 25 PCR cycles (30 s at 94 °C, 30 s at 50 °C, and 2.5 min at 72 °C)²⁷. The sequences of primers are described in the Supplementary Table 1.

Cell cycle analysis and CFSE dilution assay. The cell cycle analysis was performed with the use of Click-iT Plus EdU Alexa Fluor 647 kit (ThermoFisher Scientific). EdU is the modified analog of thymidine and gets incorporated into newly synthesized DNA. In brief, purified spleen B cells from CD19-cre Usp22 KO or WT littermates were stimulated with LPS for 3 days, before pulsing with Edu for 4 h. The cells were fixed with 4% formaldehyde, permeabilized with Perm buffer, and stained with Click-it reaction cocktail. After washing, the cells were treated with 100 µg/mL RNAse A for 10 min and then stained with PI. The stained cells were acquired on a BD LSRFortessa X-20 flow cytometer and analyzed by FlowJo software.

For CFSE dilution assay, purified spleen B cells were pulsed with 5 µM CFSE (Celltrace, Life Technologies), washed, and cultured in the presence of LPS plus IL-4. Cells were collected 4 days after CFSE pulsing and IgG1 CSR stimulation, stained with PE anti-mouse IgG1, and acquired with a BD LSRFortessa X-20 flow cytometer and analyzed by FlowJo software. The concentration of pulsed CFSE decreases as the cells divide, and thus the intensity of CFSE reflects the stages of cell division.

γH2AX immunofluorescence staining. Spleen B cells were purified from CD19-cre Usp22 KO or WT littermates, and stimulated with LPS for 2.5 days, before 0 or 8 Gy γ-irradiation (Gammacell 1000). At 1 h or 4 h post irradiation, the LPS-stimulated cells were cytospin onto poly-L-lysine slides, followed by Triton X-100 permeabilization. The slides were blocked with 10% BSA (BioShop) plus goat F(ab) polyclonal antibody against mouse IgG (Abcam, catalog number: ab6668; 1/100 dilution), to decrease nonspecific staining. The γH2AX staining using mouse monoclonal antibody against γH2AX (Millipore, clone: JBW301, catalog number: 05-636; 1/250 dilution) and quantification of foci formation were performed as we previously described¹⁴.

Germline transcripts and switch junction analysis. For germline transcript PCR, splenic B cells from CD19-cre Usp22 KO or WT mice were induced for IgG1 or IgA CSR ex vivo for 2 days. RNA was extracted and cDNA was synthesized as described above. Semi-quantitative PCR was employed to amplify Iµ-Cµ, Iγ1-Cγ1, and Ia-Cα germline transcripts using the primers as previously described⁴, and GAPDH was used as an internal control¹⁴.

For switch junction analysis, spleen B cells from CD19-cre Usp22 KO or WT littermates were induced for IgG1 or IgA CSR ex vivo for 4 days. Genomic DNA from these cells was extracted by chloroform/isopropanol and precipitated by ethanol. Switch µ-α and µ-γ1 junctions were PCR amplified with Q5 polymerase (New England Biolabs) using primers as we and others described^{14,58}, then

subsequently cloned using Zero Blunt TOPO (Life Technologies). Sequencing was carried out at The Centre for Applied Genomics (Toronto, Canada), and switch junction sequences were analyzed as we previously described¹⁴. To quantify AID activity at switch regions, we repeated the same procedure for switch junction analysis but instead using primers targeting the region upstream of switch µ or γ1.

Switch region homology analysis. Mouse immunoglobulin gene sequences for C57BL/6 were obtained from NCBI database (NC_000078.6 Ch12 and GRCm38.p4 C57BL/6 J) and the switch regions, based on their highly repetitive nature were defined by dotplot analysis using the DNASTar software (percentage: 60 or 70, Window: 30 bp, Min Quality: 1). Switch regions for BALB/c mice were described previously⁵⁹. The sequence homology of µ and downstream switch regions of C57BL/6 and BALB/c background mice were subsequently compared by the dot-plot analysis (percentage: 50–90, Window: 30 bp, Min Quality: 1).

Statistical analysis. Data were presented as mean ± SEM and were analyzed using two-tailed unpaired Student's *t*-test or two-way analysis of variance as indicated. **p* < 0.05, ***p* < 0.01, and ****p* < 0.001.

Data availability. The data that support the findings of this study are available from the corresponding author upon request.

Received: 16 October 2017 Accepted: 15 February 2018

Published online: 08 March 2018

References

- Schatz, D. G. & Ji, Y. Recombination centres and the orchestration of V(D)J recombination. *Nat. Rev. Immunol.* **11**, 251–263 (2011).
- Maizels, N. Immunoglobulin gene diversification. *Annu. Rev. Genet.* **39**, 23–46 (2005).
- Casellas, R. et al. Mutations, kataegis and translocations in B cells: understanding AID promiscuous activity. *Nat. Rev. Immunol.* **16**, 164–176 (2016).
- Muramatsu, M. et al. Class switch recombination and hypermutation require activation-induced cytidine deaminase (AID), a potential RNA editing enzyme. *Cell* **102**, 553–563 (2000).
- Rush, J. S., Fugmann, S. D. & Schatz, D. G. Staggered AID-dependent DNA double strand breaks are the predominant DNA lesions targeted to S µ in Ig class switch recombination. *Int. Immunol.* **16**, 549–557 (2004).
- Petersen, S. et al. AID is required to initiate Nbs1/γH2AX focus formation and mutations at sites of class switching. *Nature* **414**, 660–665 (2001).
- Fradet-Turcotte, A. et al. 53BP1 is a reader of the DNA-damage-induced H2A Lys 15 ubiquitin mark. *Nature* **499**, 50–54 (2013).
- Di Virgilio, M. et al. Rif1 prevents resection of DNA breaks and promotes immunoglobulin class switching. *Science* **339**, 711–715 (2013).
- Han, L. & Yu, K. Altered kinetics of nonhomologous end joining and class switch recombination in ligase IV-deficient B cells. *J. Exp. Med.* **205**, 2745–2753 (2008).
- Yan, C. T. et al. IgH class switching and translocations use a robust non-classical end-joining pathway. *Nature* **449**, 478–482 (2007).
- Boboila, C., Alt, F. W. & Schwer, B. Classical and alternative end-joining pathways for repair of lymphocyte-specific and general DNA double-strand breaks. *Adv. Immunol.* **116**, 1–49 (2012).
- Lee-Theilen, M., Matthews, A. J., Kelly, D., Zheng, S. & Chaudhuri, J. CtIP promotes microhomology-mediated alternative end joining during class-switch recombination. *Nat. Struct. Mol. Biol.* **18**, 75–79 (2011).
- Hu, H. & Sun, S. C. Ubiquitin signaling in immune responses. *Cell. Res.* **26**, 457–483 (2016).
- Ramachandran, S. et al. The SAGA deubiquitination module promotes DNA repair and class switch recombination through ATM and DNAPK-mediated γH2AX formation. *Cell Rep.* **15**, 1554–1565 (2016).
- Lang, G. et al. The tightly controlled deubiquitination activity of the human SAGA complex differentially modifies distinct gene regulatory elements. *Mol. Cell. Biol.* **31**, 3734–3744 (2011).
- Moyal, L. et al. Requirement of ATM-dependent monoubiquitylation of histone H2B for timely repair of DNA double-strand breaks. *Mol. Cell.* **41**, 529–542 (2011).
- Fierz, B. et al. Histone H2B ubiquitylation disrupts local and higher-order chromatin compaction. *Nat. Chem. Biol.* **7**, 113–119 (2011).
- Nakamura, M. et al. High frequency class switching of an IgM+ B lymphoma clone CH12F3 to IgA+ cells. *Int. Immunol.* **8**, 193–201 (1996).
- Lin, Z. et al. USP22 antagonizes p53 transcriptional activation by deubiquitinating Sirt1 to suppress cell apoptosis and is required for mouse embryonic development. *Mol. Cell.* **46**, 484–494 (2012).

20. Rickert, R. C., Roes, J. & Rajewsky, K. B lymphocyte-specific, Cre-mediated mutagenesis in mice. *Nucleic Acids Res.* **25**, 1317–1318 (1997).
21. Moor, K. et al. High-avidity IgA protects the intestine by enchaining growing bacteria. *Nature* **544**, 498–502 (2017).
22. Boulianne, B. et al. AID and caspase 8 shape the germinal center response through apoptosis. *J. Immunol.* **191**, 5840–5847 (2013).
23. Sun, T. et al. Intestinal Batf3-dependent dendritic cells are required for optimal antiviral T-cell responses in adult and neonatal mice. *Mucosal Immunol.* **10**, 775–788 (2017).
24. Lopatin, U., Blutt, S. E., Conner, M. E. & Kelsall, B. L. Lymphotoxin alpha-deficient mice clear persistent rotavirus infection after local generation of mucosal IgA. *J. Virol.* **87**, 524–530 (2013).
25. Hobeika, E. et al. Testing gene function early in the B cell lineage in mb1-cre mice. *Proc. Natl Acad. Sci. USA* **103**, 13789–13794 (2006).
26. Hardy, R. R., Carmack, C. E., Shinton, S. A., Kemp, J. D. & Hayakawa, K. Resolution and characterization of pro-B and pre-pro-B cell stages in normal mouse bone marrow. *J. Exp. Med.* **173**, 1213–1225 (1991).
27. Hesslein, D. G. et al. Pax5 is required for recombination of transcribed, acetylated, 5' IgH V gene segments. *Genes Dev.* **17**, 37–42 (2003).
28. Ehlich, A., Martin, V., Muller, W. & Rajewsky, K. Analysis of the B-cell progenitor compartment at the level of single cells. *Curr. Biol.* **4**, 573–583 (1994).
29. Daniel, J. A. et al. Deubiquitination of histone H2B by a yeast acetyltransferase complex regulates transcription. *J. Biol. Chem.* **279**, 1867–1871 (2004).
30. Cha, H. et al. Wip1 directly dephosphorylates gamma-H2AX and attenuates the DNA damage response. *Cancer Res.* **70**, 4112–4122 (2010).
31. Taccioli, G. E. et al. Impairment of V(D)J recombination in double-strand break repair mutants. *Science* **260**, 207–210 (1993).
32. Pan-Hammarstrom, Q. et al. Impact of DNA ligase IV on nonhomologous end joining pathways during class switch recombination in human cells. *J. Exp. Med.* **201**, 189–194 (2005).
33. Bjorkman, A. et al. DNA-PKcs is involved in Ig class switch recombination in human B cells. *J. Immunol.* **195**, 5608–5615 (2015).
34. Bothmer, A. et al. 53BP1 regulates DNA resection and the choice between classical and alternative end joining during class switch recombination. *J. Exp. Med.* **207**, 855–865 (2010).
35. Bromberg, K. D. et al. The SUV4-20 inhibitor A-196 verifies a role for epigenetics in genomic integrity. *Nat. Chem. Biol.* **13**, 317–324 (2017).
36. Manis, J. P. et al. 53BP1 links DNA damage-response pathways to immunoglobulin heavy chain class-switch recombination. *Nat. Immunol.* **5**, 481–487 (2004).
37. Ghazzaoui, N., Issaoui, H., Saintamand, A., Boyer, F. & Denizot, Y. Analysis of IgD CSR junctions by high-throughput sequencing. *Immunol. Lett.* **188**, 86–88 (2017).
38. Issaoui, H., Ghazzaoui, N., Saintamand, A., Denizot, Y. & Boyer, F. IgD class switch recombination is not controlled through the immunoglobulin heavy chain 3' regulatory region super-enhancer. *Cell. Mol. Immunol.* **14**, 871–874 (2017).
39. Zhang, X. Y., Pfeiffer, H. K., Thorne, A. W. & McMahon, S. B. USP22, an hSAGA subunit and potential cancer stem cell marker, reverses the polycomb-catalyzed ubiquitylation of histone H2A. *Cell Cycle* **7**, 1522–1524 (2008).
40. Zhao, Y. et al. A TIFC/STAGA module mediates histone H2A and H2B deubiquitination, coactivates nuclear receptors, and counteracts heterochromatin silencing. *Mol. Cell.* **29**, 92–101 (2008).
41. Atanassov, B. S. et al. ATXN7L3 and ENY2 coordinate activity of multiple H2B deubiquitinases important for cellular proliferation and tumor growth. *Mol. Cell.* **62**, 558–571 (2016).
42. Nutt, S. L., Urbanek, P., Rolink, A. & Busslinger, M. Essential functions of Pax5 (BSAP) in pro-B cell development: difference between fetal and adult B lymphopoiesis and reduced V-to-DJ recombination at the IgH locus. *Genes Dev.* **11**, 476–491 (1997).
43. Corcoran, A. E., Riddell, A., Krooshoop, D. & Venkitaraman, A. R. Impaired immunoglobulin gene rearrangement in mice lacking the IL-7 receptor. *Nature* **391**, 904–907 (1998).
44. Difilippantonio, S. et al. 53BP1 facilitates long-range DNA end-joining during V(D)J recombination. *Nature* **456**, 529–533 (2008).
45. Bjorkman, A. et al. Reduced immunoglobulin gene diversity in patients with Cornelia de Lange syndrome. *J. Allergy Clin. Immunol.* **141**, 408–411 (2018).
46. Slack, E., Balmer, M. L. & Macpherson, A. J. B cells as a critical node in the microbiota-host immune system network. *Immunol. Rev.* **260**, 50–66 (2014).
47. Levy, M., Kolodziejczyk, A. A., Thaiss, C. A. & Elinav, E. Dysbiosis and the immune system. *Nat. Rev. Immunol.* **17**, 219–232 (2017).
48. Belcheva, A. et al. Gut microbial metabolism drives transformation of MSH2-deficient colon epithelial cells. *Cell* **158**, 288–299 (2014).
49. Arnold, L. W., Grdina, T. A., Whitmore, A. C. & Houghton, G. Ig isotype switching in B lymphocytes. Isolation and characterization of clonal variants of the murine Ly-1+ B cell lymphoma, CH12, expressing isotypes other than IgM. *J. Immunol.* **140**, 4355–4363 (1988).
50. Kaminski, D. A. & Stavnezer, J. Enhanced IgA class switching in marginal zone and B1 B cells relative to follicular/B2 B cells. *J. Immunol.* **177**, 6025–6029 (2006).
51. Kim, A., Han, L., Santiago, G. E., Verdun, R. E. & Yu, K. Class-switch recombination in the absence of the IgH 3' regulatory region. *J. Immunol.* **197**, 2930–2935 (2016).
52. Issaoui, H. et al. The IgH 3' regulatory region super-enhancer does not control IgA class switch recombination in the B1 lineage. *Cell Mol. Immunol.* **14**, 1–3 (2017).
53. Macpherson, A. J. et al. IgA production without mu or delta chain expression in developing B cells. *Nat. Immunol.* **2**, 625–631 (2001).
54. Li, S. K., Solomon, L. A., Fulkerson, P. C. & DeKoter, R. P. Identification of a negative regulatory role for spi-C in the murine B cell lineage. *J. Immunol.* **194**, 3798–3807 (2015).
55. Pinaud, E. et al. Localization of the 3' IgH locus elements that effect long-distance regulation of class switch recombination. *Immunity* **15**, 187–199 (2001).
56. Guikema, J. E. et al. APE1- and APE2-dependent DNA breaks in immunoglobulin class switch recombination. *J. Exp. Med.* **204**, 3017–3026 (2007).
57. Larjani, M. et al. Lack of MSH2 involvement differentiates V(D)J recombination from other non-homologous end joining events. *Nucleic Acids Res.* **33**, 6733–6742 (2005).
58. Begum, N. A. et al. Requirement of non-canonical activity of uracil DNA glycosylase for class switch recombination. *J. Biol. Chem.* **282**, 731–742 (2007).
59. Pan-Hammarstrom, Q., Zhao, Y. & Hammarstrom, L. Class switch recombination: a comparison between mouse and human. *Adv. Immunol.* **93**, 1–61 (2007).

Acknowledgements

We thank the Martin lab members for their advice and discussion during this study, Dr Stephen Li for the help in B-cell profiling analysis by flow cytometry, Dr Michael Reth for the Mb1-Cre mice, to Dr Daniel Durocher for the 53BP1^{-/-} mice. C.L. is a recipient of the Canadian Institutes of Health Research Postdoctoral Fellowship. This research is supported by a grant from the Canadian Institutes of Health Research (Grant number PJT153307) to A.M.

Author Contributions

C.L. designed the experiments, performed the research, analyzed data, and wrote the manuscript. T.I., C.S., M.B., E.L., and A.L. performed the research. Q.P., L.D., and J.L.G. analyzed data and edited the manuscript. A.M. designed the experiments, analyzed data, and wrote the manuscript.

Additional information

Supplementary Information accompanies this paper at <https://doi.org/10.1038/s41467-018-03455-x>.

Competing interests: The authors declare no competing interests.

Reprints and permission information is available online at <http://npg.nature.com/reprintsandpermissions/>

Publisher's note: Springer Nature remains neutral with regard to jurisdictional claims in published maps and institutional affiliations.



Open Access This article is licensed under a Creative Commons Attribution 4.0 International License, which permits use, sharing, adaptation, distribution and reproduction in any medium or format, as long as you give appropriate credit to the original author(s) and the source, provide a link to the Creative Commons license, and indicate if changes were made. The images or other third party material in this article are included in the article's Creative Commons license, unless indicated otherwise in a credit line to the material. If material is not included in the article's Creative Commons license and your intended use is not permitted by statutory regulation or exceeds the permitted use, you will need to obtain permission directly from the copyright holder. To view a copy of this license, visit <http://creativecommons.org/licenses/by/4.0/>.

© The Author(s) 2018